

Functional insights from molecular modeling, docking, and dynamics study of a cypoviral RNA dependent RNA polymerase



Anirban Kundu, Anirudha Dutta, Poulomi Biswas, Amit Kumar Das,
Ananta Kumar Ghosh*

Department of Biotechnology, Indian Institute of Technology Kharagpur, Kharagpur 721302, India

ARTICLE INFO

Article history:

Received 30 April 2015

Received in revised form 27 June 2015

Accepted 18 July 2015

Available online 26 July 2015

Keywords:

Anthraea mylitta

Cytoplasmic polyhedrosis virus

Double stranded RNA virus

RNA dependent RNA polymerase

Molecular modeling

Docking and simulation

ABSTRACT

Anthraea mylitta cytoplasmic polyhedrosis virus (AmCPV) contains 11 double stranded RNA genome segments and infects tasar silkworm *A. mylitta*. RNA-dependent RNA polymerase (RdRp) is reported as a key enzyme responsible for propagation of the virus in the host cell but its structure function relationship still remains elusive. Here a computational approach has been taken to compare sequence and secondary structure of AmCPV RdRp with other viral RdRps to identify consensus motifs. Then a reliable pairwise sequence alignment of AmCPV RdRp with its closest sequence structure homologue λ3 RdRp is done to predict three dimensional structure of AmCPV RdRp. After comparing with other structurally known viral RdRps, important sequence and/or structural features involved in substrate entry or binding, polymerase reaction and the product release events have been identified. A conserved RNA pentanucleotide (5'-AGACG-3') at the 3'-end of virus genome is predicted as *cis*-acting signal for RNA synthesis and its docking and simulation study along with the model of AmCPV RdRp has allowed to predict mode of template binding by the viral polymerase. It is found that template RNA enters into the catalytic center through nine sequence-independent and two sequence-dependent interactions with the specific amino acid residues. However, number of sequence dependent interactions remains almost same during 10 nano-second simulation time while total number of interactions decreases. Further, docking of N⁷-methyl-GpppG (mRNA cap) on the model as well as prediction of RNA secondary structure has shown the template entry process in the active site. These findings have led to postulate the mechanism of RNA-dependent RNA polymerization process by AmCPV RdRp. To our knowledge, this is the first report to evaluate structure function relationship of a cypoviral RdRp.

© 2015 Elsevier Inc. All rights reserved.

1. Introduction

Anthraea mylitta cytoplasmic polyhedrosis virus (AmCPV) is a potent threat of Indian non-mulberry silkworm, *A. mylitta*. CPV-infected *A. mylitta* larvae develop chronic diarrhea, namely, "Grasserie" which leads to the death of the larvae [1]. CPV belongs to the genus *Cypovirus* of the family Reoviridae [2] and contains 10–11 double stranded RNA segments in its genome [3–5]. Each dsRNA segment is composed of a plus strand mRNA and its complementary minus strand in an end to end base pair configuration except for a protruding 5' cap on the plus strand. Our laboratory has previously characterized AmCPV by electron microscopy and its genome by electrophoresis, which revealed that it is similar to that of type-4CPV and consists of eleven segmented (S1–S11) double

stranded RNA (dsRNA) molecules [6]. Molecular characterization of all these genome segments and elucidation of their functions [7–14] have shown that S2 of AmCPV codes for RNA dependent RNA polymerase (RdRp) responsible for replication/transcription [15]. But the structural basis of its enzymatic activity is still unclear.

The RdRp is an essential protein encoded by all RNA viruses except retroviruses, which catalyzes phosphodiester-bond formation between two ribonucleotides (NTPs) in a RNA template-dependent fashion. These enzymes can function alone or need other viral proteins for their optimum activity [16,17]. Unlike other virus families, segmented dsRNA viruses of the Reoviridae family possess multiple copies of RdRps anchored inside the icosahedral viral core shell, slightly off-centered from each fivefold axis. Each RdRp is associated with one of the 10–12 dsRNA genome segments for efficient recruitment of RNA template strands throughout the infection cycle [17–19]. During viral transcription, Reoviridae RdRp participates multiple round of plus strand (+) RNA synthesis using minus strand (-) RNA of dsRNA as template within a confined proteina-

* Corresponding author. Fax: +91 3222 278707.

E-mail address: aghosh@hjli.iitkgp.ernet.in (A.K. Ghosh).

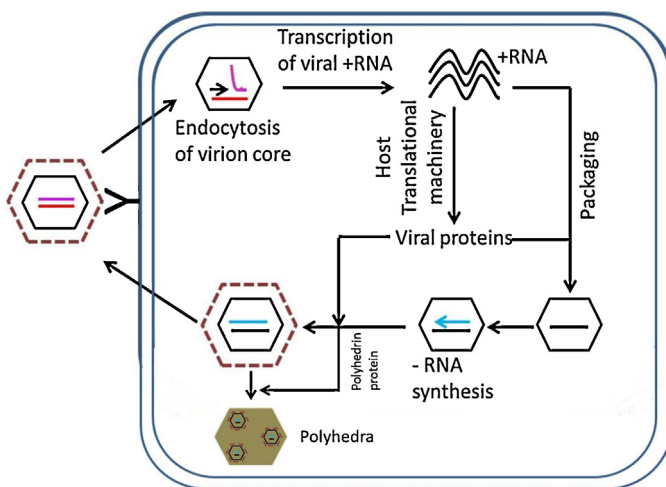


Fig. 1. Schematic diagram of transcription/replication cycle of CPV. After viral entry into the host cell by receptor mediated endocytosis, the outer capsid layer are removed and a virion core of inner capsid layer containing dsRNA genome are released into the cytoplasm. The core transcribes plus strand RNAs by the viral RdRp and extrudes them. They are then translated and packaged by the resulting viral proteins into new virion cores. Mature cores are formed by synthesizing negative strand RNA (cyan colored arrow) by viral RdRp and outer capsid layer, and then comes out of the cell or formed polyhedra inside the cells.

ceous viral core. The newly synthesized (+) RNA comes into the host cell cytoplasm following RNA capping machinery of the virus and produces viral proteins using host translational machinery. It is followed by packaging of the (+) RNAs into viral core particle and during the assembly procedure, RdRp initiates a single round (−) RNA synthesis on each (+) RNA so that each viral progeny particle can have a complete constellation of genome segments (Fig. 1). Review of the available sequences has revealed that beyond several conserved motifs, very low sequence similarities are present among the RdRps from different virus families and within the different genera of the same virus family as well. However, the analysis of available crystal structures has shown that there are remarkable structural similarities present among the viral RdRps including RdRps from reovirus ($\lambda 3$) and rotavirus (VP1) which are only two structurally known polymerases from the family Reoviridae [20].

They all have adopted typical polymerase structure of right handed shape formed by fingers, palm and thumb subdomains. One of the distinct structural features that separate $\lambda 3$ RdRp or rotavirus VP1 from RdRps of the other viral families is that their right handed polymerase domain (PD) is sandwiched by a large N-terminal domain (NTD) and a large C-terminal domain (CTD), forming a globular cage like structure with a buried catalytic center connected to the exterior of the protein by four distinct channels which are responsible for substrate(s) entry and product(s) release. Soaking of biologically relevant RNA oligonucleotide with $\lambda 3$ RdRp or VP1 crystals has revealed that in crystal packing $\lambda 3$ RdRp mimics the transcription mode of RNA synthesis whereas VP1 emulates a Reoviridae RdRp before packaging [21,22]. In case of blue tongue virus (BTV), another member of the Reoviridae family, segment 1 encoded purified VP1 protein can act as the BTV replicase (RdRp) synthesizing dsRNA from viral plus strand RNA template in the absence of any other virus encoded protein [23]. A structural model of BTV RdRp generated by *in silico* analysis has shown that it also contains three domains and its PD structure as right hand, complete with fingers, palm and thumb sub-domains like rotavirus VP1 and $\lambda 3$ RdRp [24]. However, its overall secondary structural organization is rather different from other RdRps. CPV is the simplest member of the Reoviridae family in terms of having single capsid layer which shelters all the enzymes required for an efficient infection [25]. CPV can be consid-

ered as “turreted” subgroup of the Reoviridae because of presence of a pentameric turret formed by five copies of turret proteins on fivefold vertex of the innermost shell, which functions in the catalysis of mRNA 5' cap synthesis [26–29]. Recent cryo-EM structures of transcribing and non-transcribing BmCPV have mapped the post-transcriptional processing pathway of newly transcribed +RNA [29–31]. However, the mechanism of genomic RNA synthesis and assembly of dsRNA within the virus core particle have not been studied in detail for any CPV. In comparison to other members of the Reoviridae family, CPV RdRp is presumed to have a key involvement in the genomic RNA synthesis and packaging of virus core particles [15,27,32,33]. As evidenced from rotavirus and $\lambda 3$ RdRp, in spite of having remarkable similarities in overall architectures, they exhibit some differences that explain how individual genera within a same virus family mediate RNA synthesis. Hence, it is worthwhile to study structure–function relationship of cypoviral RdRPs.

Given the crucial role of RdRp in virus life cycle and the absence of any structural data and very limited biochemical data on cypoviral RdRPs, here, we have taken *in silico* approach to decipher structure–function relationship of AmCPV RdRp. A stepwise protocol has been designed to model structure of AmCPV RdRp. Based on sequence and/or structure comparison we describe potential roles of specific residues in the polymerization mechanism and can explain structural basis of some of the important biochemical data available for AmCPV RdRp. Further, docking and/or simulation analysis of AmCPV RdRp model with the template RNA and the mRNA cap have enabled us to address possible mechanism of RNA synthesis by the polymerase. The analysis is likely to provide guidance in the design of future biochemical experiments and aid in the development of anti-AmCPV agents. To our knowledge, this is the first attempt aimed at evaluation of the structure–function relationship of a cypoviral RdRp.

2. Materials and methods

2.1. Sequence alignment and homology model building

AmCPV RdRp (1116 amino acid residues; GeneBank accession number: GQ351286) shares moderate sequence identity with other cypoviral RdRPs but has very low sequence similarity with other viral RdRPs of known structures. Therefore, any conventional method of sequence alignment was not supportive. As homology modeling depends on authentic alignment to the sequence of a known structure, polymerase modeling was hampered by low sequence homology. Hence, we carried out a systematic approach to obtain a satisfactory homology model of the viral polymerase and the scheme is depicted in Fig. 2. An initial structure of AmCPV RdRp was predicted using an *ab initio* structure prediction methodology, I-TASSER which predicts 3D structure of protein based on multiple-threading alignments and the iterative implementation of the threading assembly refinement [34]. Further, Sequence of AmCPV RdRp was aligned with other cypoviral RdRPs and two representatives of known crystal structures of the family Reoviridae using program MAFFT (<http://mafft.cbrc.jp/alignment/server/>) with E-INS-i strategy which supports alignment of sequences with several conserved motifs embedded in long unalignable regions (Fig. S1). The cypoviruses used in sequence alignment were from *Choristoneura occidentalis* (CoCPV; GeneBank accession no. ACA53380.1), *Dendrolimus punctatus* (DpCPV; GeneBank accession no. AAN46860.1), and *Bombyx mori* (BmCPV; GeneBank accession no. AAK20302.1). Rotavirus VP1 (PDB 2R7O) and reovirus $\lambda 3$ RdRp (PDB 1N35) were used as guide in the sequence alignment to identify probable domain boundaries and conserved sequence motifs present in AmCPV RdRp and other cypoviral RdRPs. Then the align-

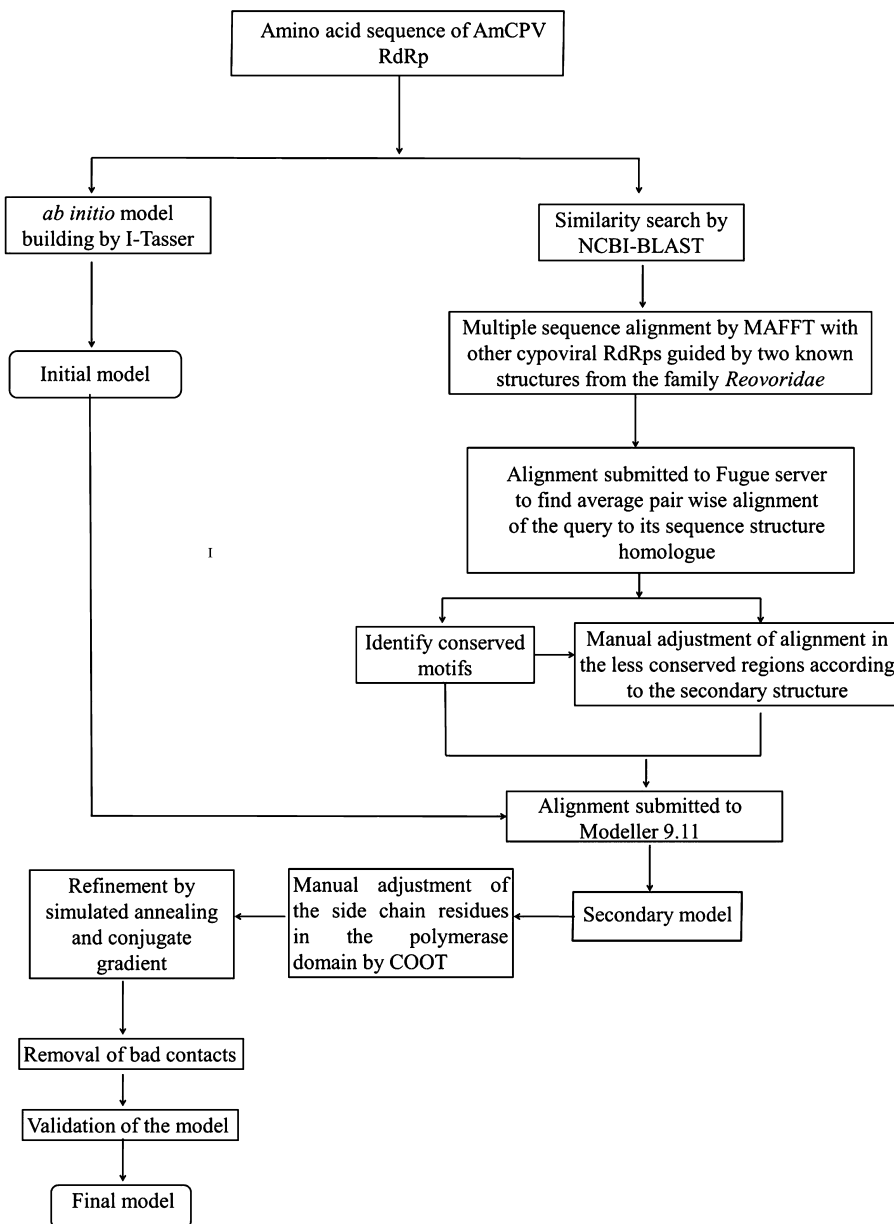


Fig. 2. Scheme for prediction of three dimensional structure of AmCPV RdRp.

ment was submitted to FUGUE server (<http://tardis.nibio.no.jp/fugue/prfsearch.html>) to obtain an average pair wise alignment of the query to its best (Z score = 64) sequence structure homologue that was structure of λ3 RdRp (PDB 1N35). Subsequently, PSIPRED (<http://bioinf.cs.ucl.ac.uk/psipred/>) and CFSSP, Chou & Fasman Secondary Structure Prediction Server (<http://www.biogem.org/cgi-bin/cho-fas.pl>) were used to predict secondary structure of AmCPV RdRp. Then the alignment was optimized manually according to the previous knowledge of domains and consensus sequences found in RdRps of known structures and secondary structure comparison with λ3 RdRp. Finally the adjusted alignment along with the I-TASSER generated *ab initio* model was submitted to the software MODELLER v9.11 [35] to generate a more authentic three-dimensional model of AmCPV RdRp based on the coordinates of amino acids from the crystal structure of λ3 RdRp (PDB 1N35). The derived model was inspected manually for orientations of the side chains of the conserved residues in the consensus motifs. Crystal structures of RdRps from λ3 (PDB 1N35, 1MUK, 1N38, and 1N1H), Rotavirus (PDB 2R7O), polio virus (PV) (PDB 1RDR), Hep-

atitis C Virus (HCV) (PDB 1QUV), and Rabbit hemorrhagic disease virus (RHDV) (PDB 1KHV) were taken as guidance for the visual inspection. Any change in the side chain orientation was made in COOT [36] considering alternative favorable rotamers of the side chain. The model was further optimized by very slow and accurate refinement protocol using conjugate gradients and simulated annealing methods available with MODELLER package. The bad contacts in the model were removed by What IF server (<http://swift.cmbi.ru.nl/servers/html/index.html>). The quality of the final model was evaluated by the program PROCHECK [37]. Representation of sequence alignment and molecular structure was made by ESPript v3.0 (<http://escript.ibcp.fr/ESPrift/ESPrift/>) Pymol molecular graphics system (Schrödinger, LLC), respectively.

2.2. Docking of N⁷-methyl-guanosine mRNA cap (N⁷-mGpppG) in modeled AmCPV RdRp

The 3D model of AmCPV RdRp was used as a target receptor for docking of N⁷-methyl-GpppG cap. The AutoDock Vina software

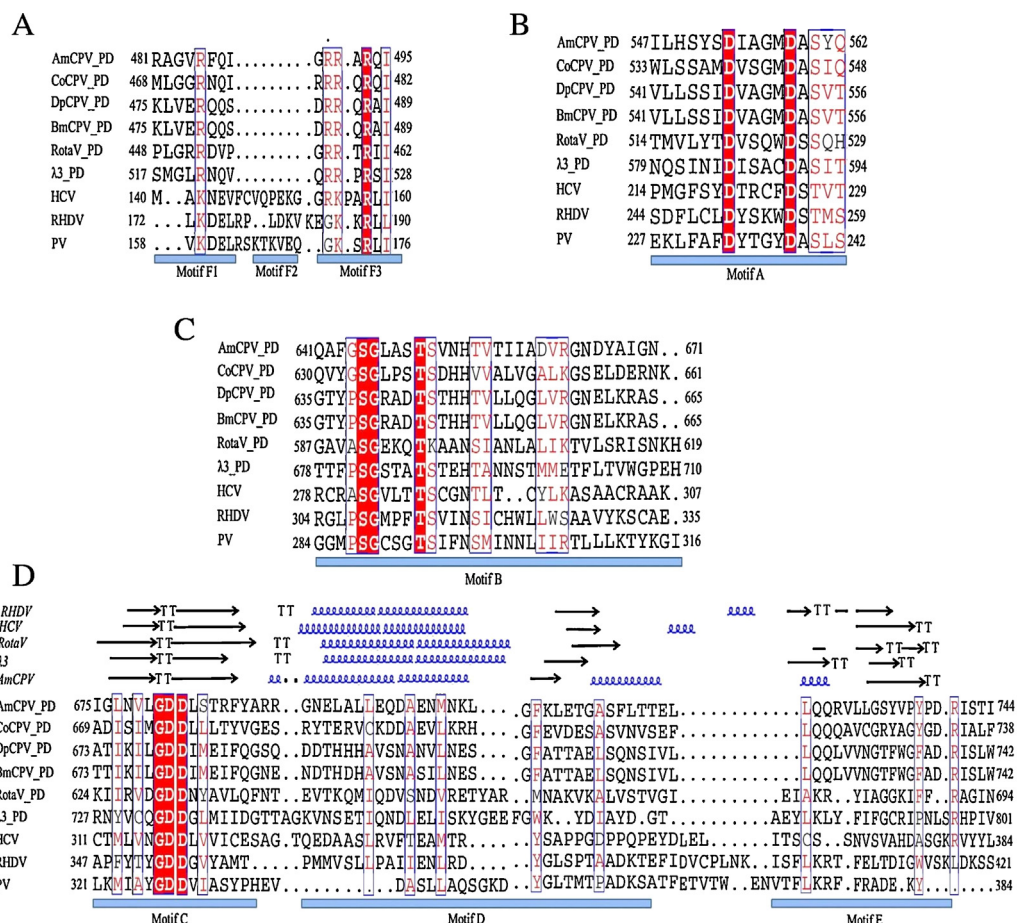


Fig. 3. Alignment in the regions of six conserved motifs (A–F) extracted from multiple sequence alignment of the polymerase domain (PD) of AmCPV RdRp (Fig. S2) (GQ351286). The representative cytopathic RdRPs in the alignment are from: CoCPV (ACA53380.1), DpCPV (AAN46860.1), and BmCPV (AAK20302.1). Five structural representatives in the alignment are $\lambda 3$ (PDB 1N35), rotavirus (RotaV) (PDB 2R7O), PV (PDB 1RDR), HCV (PDB 1QUV), and RHDV (PDB 1KHV). Motifs A, B, C, and F can be aligned confidently among different viral RdRPs, however, sequence in the motifs D and E are less conserved and aligned through the help of secondary structure alignment. Secondary structures of the structural representatives are extracted from their corresponding PDB files. Invariant residues are highlighted in red fill box while conserved residues are red. Motifs are highlighted with blue bar. α -helices are shown in spirals, β -strands as arrows and turns as TT. (For interpretation of the references to color in this figure legend, the reader is referred to the web version of this article.)

package [38] was used to dock the compound with a grid spacing of 1 Å and exhaustiveness of 48, and PyMol (Schrödinger) was used to analyze the data. The coordinate of the ligand molecule was prepared from PRODRG server (<http://davapc1.bioc.dundee.ac.uk/cgi-bin/prodrg>). Then the receptor molecule was protonated by adding polar hydrogens. The receptor was kept rigid while all the torsional bonds of the ligand were set free to rotate. The docking area of mRNA cap was set by a grid box of dimensions $32 \times 24 \times 36$ Å³ near the predicted template entry tunnel according to the cap binding site of rotavirus and $\lambda 3$ RdRp. The docking search produced a ranked list of receptor–ligand interactions with binding free energy values. The best orientation of the ligand molecule was selected according to the free energy value and previous knowledge of binding mode studied elsewhere [21,39].

2.3. RNA secondary structure prediction

Secondary structure prediction was accomplished by Mfold web server v3.0 (<http://mfold.rna.albany.edu/?q=mfold>). Mfold predicts secondary structure on the basis of free energy minimization using dynamic programming algorithm as described by Zuker [40]. Briefly, a set of suboptimal structures are generated from a given sequence within a variation of 20% of free energy from the lowest free energy. Then coaxial stacking rule and theory of multi-branched loops are used through efn2 algorithm to recalculate free

energy of the predicted structures thereby reordering them according to stability.

2.4. Protein–RNA docking

Most of the AmCPV mRNAs (+RNA) contain 5'-AGAGC-3' sequence at their 3' termini. The coordinate of terminal pentanucleotides (5'-AGAGC-3') of (+) strand RNA was obtained by extracting coordinate of RNA molecule from the short initiation complex of $\lambda 3$ RdRp (PDB 1N38) which contained 5'-UUAGC-3' as bound RNA and mutated at the positions of initial two nucleotides (underlined) in COOT. Then the RNA pentanucleotide was docked in RdRp model by the program HEX [41] first considering a rigid body prediction with the RNA ligand oriented towards predicted template entry tunnel. Subsequently, only shape and shape-electrostatics correlation algorithms were used with a search radius of $n = 28$, and top ten models were inspected visually in COOT. In order to increase the docking approximation of the RNA molecule, MODELLER (v9.12) program was also used to dock the terminal conserved pentanucleotides (5'-AGAGC-3') in the model structure. For this, short elongation complex of $\lambda 3$ RdRp (1N38) was taken as template and modified. Modified 1N38 contained terminal pentanucleotides of AmCPV RNA, prepared as described above, in its template entry tunnel and any close contacts between amino acid side chains and the RNA molecule were removed by COOT

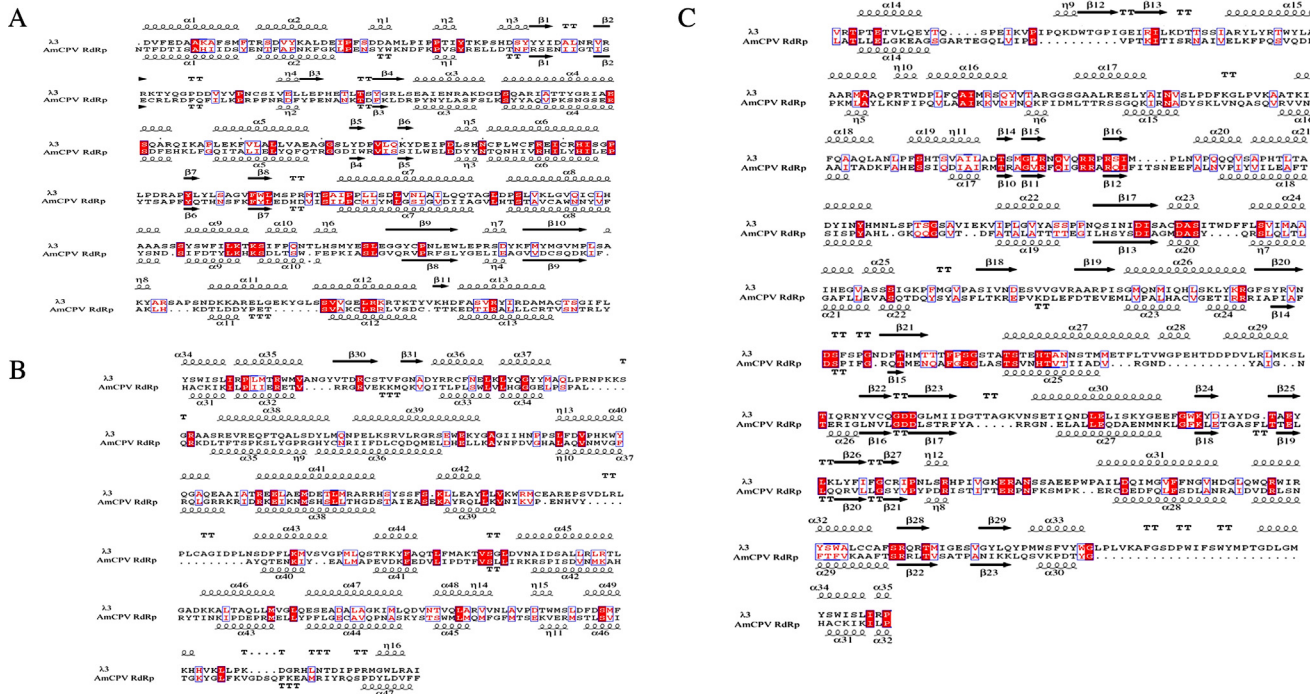


Fig. 4. Pairwise sequence-structure alignment of AmCPV RdRp (amino acid residues 10–1116) and $\lambda 3$ (PDB 1N35) (25–1221) in the regions of N-terminal (A), C-terminal (B) and the polymerase domain (C). Similar and identical residues are shaded as described for Fig. 3.

using alternative favorable rotamers of the side chains. Finally, the five lowest energy models generated by MODELLER were compared manually with top five docked structures obtained from HEX software with respect to the position of the RNA molecule in the predicted template entry tunnel as discussed by Tao et al. [21] and the best possible orientation was selected with no short contacts.

2.5. Molecular dynamic simulation in explicit solvent

Molecular dynamics simulations of the modeled RdRp and its complex with RNA were performed using GROMACS v4.5.5 software [42] package in order to investigate the effect of RNA binding on the dynamic motions model in an explicit water environment. All simulations were performed using AMBER-95 all atom force field [43]. The model RdRp or RdRp–RNA complex was placed in cubic boxes filled with TIP3P water molecules [44] and rendered electro neutrals by the addition of counter ions using the genion program of the GROMACS package that replaces solvent molecules by ions at the position with the most favorable electrostatic potential. The resulting systems contained 54,401 water molecules, 5Cl^- ions and 17,773 protein atoms for the protein only, and 55,548 water molecules, 1Cl^- ion, 17,773 protein atoms and 164 RNA atoms for RdRp–RNA complex. Initially backbone atoms of the model or the complex were constrained and the solvent molecules and the ions were allowed to optimize themselves using decreasing force constant of $1000 \text{ kJ}/(\text{mol nm})$. The systems were then simulated for 10 ns in periodic boundary conditions, at a constant temperature of 300 K using the Berendsen's method [45] and at a constant pressure of one bar maintained by Rahman–Parrinello barostat [46] and with a 2 fs time step. The electrostatic interactions were taken into account by means of the Particle Mesh Ewald method [47], using a cut-off radius of 0.9 nm in real space, while a cut-off radius of 1.4 nm was chosen for the van der Waals interactions. The lengths of all bonds were kept constant with the Lincs

algorithm [48]. All the simulations were performed on a workstation HP Z220 equipped with quad core Intel® Xeon® processor E3-1280v2. $\text{C}\alpha$ -RMSD and radius of gyration plots was generated using grace program (<http://plasma-gate.weizmann.ac.il/cgi-bin/viewvc.cgi/grace/>) to observe stability of the protein or the complex.

2.6. Electrophoretic mobility shift assay

In order to investigate the specific binding of 3' end of (+) viral RNA strand by AmCPV RdRp, the 3' end of AmCPV S2 (+) strand RNA was synthesized as minigenome as described by Ghorai et al. [15]. In brief, initially 183 bp of 3' end of AmCPV S2 was amplified by PCR from S2 cDNA using forward primer TF5 (5'- **GATTAGGTGACACTATA**GCTTCAGCCCAGGAGTACCGC-3') containing SP6 promoter sequence represented in bold and reverse primer TF6 (5'-GCTCTATACCATCCGATCGCT-3') and eluted from gel by gel extraction kit (Qiagen). Then *in vitro* transcription reaction (50 μl) was carried out using the PCR product (1 μg) as template and MAXIscript SP6 reaction Kit (Ambion) in the presence of 5 μl [α - ^{32}P] UTP of specific activity 3500 Ci/mmol. After overnight incubation, the DNA was destroyed by TURBO DNase (2U) (Ambion) and the transcripts were purified by RNeasy mini elute kit (Qiagen). Mobility shift assay was carried out in low salt buffer (5 mM Tris–HCl pH 7.1, 30 mM NaCl, and 15% glycerol), containing 1.0 μg of the labeled purified transcript (1,25,000 cpm/ μg), ~5 μg of purified recombinant AmCPV RdRp [15], 20U RNase inhibitor (NEB) and different amount of yeast tRNA (non-specific RNA). Reaction mixtures were incubated for 30 min at room temperature and the complexes formed between the labeled RNA probe and RdRp were resolved by electrophoresis on non-denaturing 8% polyacrylamide gel. The gel was dried, exposed to digital x-ray film (Fuzi) and analyzed by autoradiography (Typhoon, GE).

3. Results and discussions

3.1. Sequence comparison and homology modeling

AmCPV RdRp has ~40% sequence identity with other cypoviral RdRps. However, it shares <16% sequence identity with other viral RdRps of known structures. Such a low level of identity would not produce any reliable alignment. Hence, a step wise protocol including multiple sequence alignment and sequence-structure homologue search has been adopted to obtain an average pairwise alignment of AmCPV RdRp with its closest homologue, λ3 RdRp. Such an alignment has suggested that approximately initial 350 amino acid residues might span the N-terminal domain (NTD), 351–824 residues could form the polymerase domain (PD) and the rest (815–1116 amino acids) could cover the C-terminal domain (CTD) of AmCPV RdRp. Other members of the Reoviridae family may contain three individual domains, of which two are structurally validated [21,39]. PD is common among other viral polymerases. Hence, sequence of AmCPV PD could be compared to other viral polymerases of known structures based on previous knowledge of sub-domains and conserved motifs. However, no characteristic motifs of NTD or CTD are reported till date. Sequence comparison of PD of AmCPV, CoCPV, DpCPV, and BmCPV with that of λ3, rotavirus and HCV, PV, and RHDV polymerases has allowed to initially identify motifs A (D-X₄-D), B (SG-X₃-TS/K), C (GDD), and F (K/R-X₁₋₃-R) [49] in AmCPV PD (Fig. 3). Alignment of less conserved motifs has been aided by secondary structure comparison. After motif C, motif D is located in the region of a long α-helix followed by a β-strand. Motif D appears to contain a hydrophilic residue (E/N/S) at the C-terminus of the α-helix, and an aromatic residue (F/Y/W) in the following β turn (Fig. 3 and Fig. S2) as suggested by Xu et al. [50]. We have assigned motif D based on the alignment of a predicted α-helix after motif C in AmCPV RdRp with that of other viral RdRp structures as well as a hydrophilic residue (E) at the C-terminus of the helix and an aromatic residue (F) in the following turn. Motif E of AmCPV RdRp has been identified in the conserved β hairpin structure following motif D (Fig. 3 and Fig. S2). Identification of these motifs helped manual adjustment of the initial pairwise alignment to obtain a reliable alignment of AmCPV RdRp with the sequence of its closest sequence-structure homologue, λ3 RdRp (Fig. 4). Identification of conserved motifs and establishment of reliable alignment has helped to build a three-dimensional homology model of AmCPV RdRp based on coordinates of amino acids in the crystal structure of λ3 RdRp (PDB 1N35).

Moreover, an *ab initio* model has also been developed to facilitate optimization during template based homology modeling. The final model (Fig. 5A) consists of total 1107 amino acid residues out of 1116 residues. Initial nine residues have been omitted from the alignment map because of no sequence similarity with the template. Over 99% of the residues of the model are in allowed region of the Ramachandran plot and the overall G factor is −0.14 (Fig. S3) indicating a model of good molecular geometry. Predicted secondary structures are in good agreement with the secondary structures of the model and the Cα backbone of the model is deviated by 1.6 Å (root mean square deviation, RMSD) from the Cα backbone of the template. Analysis of the structural model has allowed us to discuss the potential functional roles of the domains, conserved motifs and specific residues in polymerization.

3.2. Structural overview of the model

The 3D-model depicts spatial organization of the three domains present in AmCPV polymerase. The organization is very similar to two other structurally known members of the Reoviridae family (λ3 and rotavirus polymerase) with some exceptions. The N- and C-terminal domains cover the central polymerase domain in

such a way that the overall structure forms a cage like architecture with a large hollow center connected by four tunnels from the surface of the molecules dedicated for rNTP entry/PPi release, template entry, ds RNA product/template release and nascent transcript release. The possible four tunnels have been predicted in the model by taking analogy from rotavirus VP1 structure (Fig. 5B) [22]. Unlike tunnels for rNTP entry/PPi release, template entry, and nascent transcript release which are comprised of parts from N-terminal and polymerase and/or C-terminal domains, the tunnel for dsRNA product/template release is exclusively made of the C-terminal domain.

3.2.1. Polymerase domain

The central polymerase domain of the model (residues 351–824) is very similar to the other viral polymerases in their three-dimensional organization by exhibiting a central cupped, right handed architecture with fingers, palm and thumb subdomains (Fig. 5D). The subdomains of the model are compared with other viral polymerases with respect to conserved motifs present among them (Fig. 6). The fingers subdomain is predicted to span approximately from residues 356 to 523 and 563 to 639. The 'base' of the fingers is mainly α-helical and the 'tip' of the fingers consists primarily of β-strands and random coils. Despite high sequence variability in the fingers subdomain of different viral RdRps, there is a conserved sequence motif, motif F, which can be predicted in AmCPV RdRp (Fig. 3A). Motif F contains several conserved basic residues and may consist of sub-motifs, F1, F2 and F3 [51]. Sub-motif F2 does not appear to present in RdRps of the Reoviridae family including λ3, rotavirus, AmCPV, BmCPV, CoCPV, and DpCPV (Fig. 3). In AmCPV RdRp, motif F3 contains several highly conserved basic amino acid residues including R485, R490, R491, and R493 which may interact with rNTP(s) and template strand as found in case of other viral RdRps [21,52,53]. Like HCV and λ3, the structural element that contains those conserved basic residues is 'β-strand, loop and β-strand', which interacts with the thumb subdomain and helps to adopt a closed conformation [21,54,55]. Recent studies on rotavirus VP1 have suggested that K419 of the fingers subdomain limits RNA entry into the template entry tunnel thereby reduces the rate of product RNA synthesis [56]. Structurally equivalent residue of K419 is R433 of the model, which is also resided in the predicted template entry tunnel and likely to serve for the same function. This fact can be correlated with the idea that moderate rate of RNA synthesis may enhance VP1 fidelity. The palm subdomain of AmCPV RdRp spans approximately from residues 524 to 562 and 640 to 742 and contains motif A–E, of which motif E is found only in RdRps and reverse transcriptases (RTs) while others are common in all polymerases [57]. These motifs are arranged in A–E amino- to carboxyl-terminal order as found in other canonical RdRps (Fig. 6) while permuted order of the motifs (C–A–B–D–E) is predominant in birnavirus, another member of dsRNA virus family [58]. Moreover, a loop containing residues 526–534 is likely to correspond to the priming loop which is unique to RdRps of Reoviridae family and is located between finger subdomain and the motif A (Fig. 5D). These motifs in together form a central four-stranded anti-parallel β-sheet flanked by three α-helices, the arrangement found in most of the viral polymerases. As in other viral polymerases, motif A is composed of a β-strand and short α-helix structure, of which two aspartic acid residues (D553 and D558) are highly conserved (Fig. 3B). Motif C has a β-hairpin structural element in all types of polymerases and two conserved aspartic acid residues are located in the turn of the hairpin structure (Fig. 3D). In case of model structure, D682 and D683 are two conserved aspartate residues of the motif C. Comparing with other viral polymerases, D558 of motif A is likely to be involved in the ribose sugar selection while D553 along with two conserved aspartic acid residues from motif C and two metal ions and water molecules are expected to catalyze phospho-

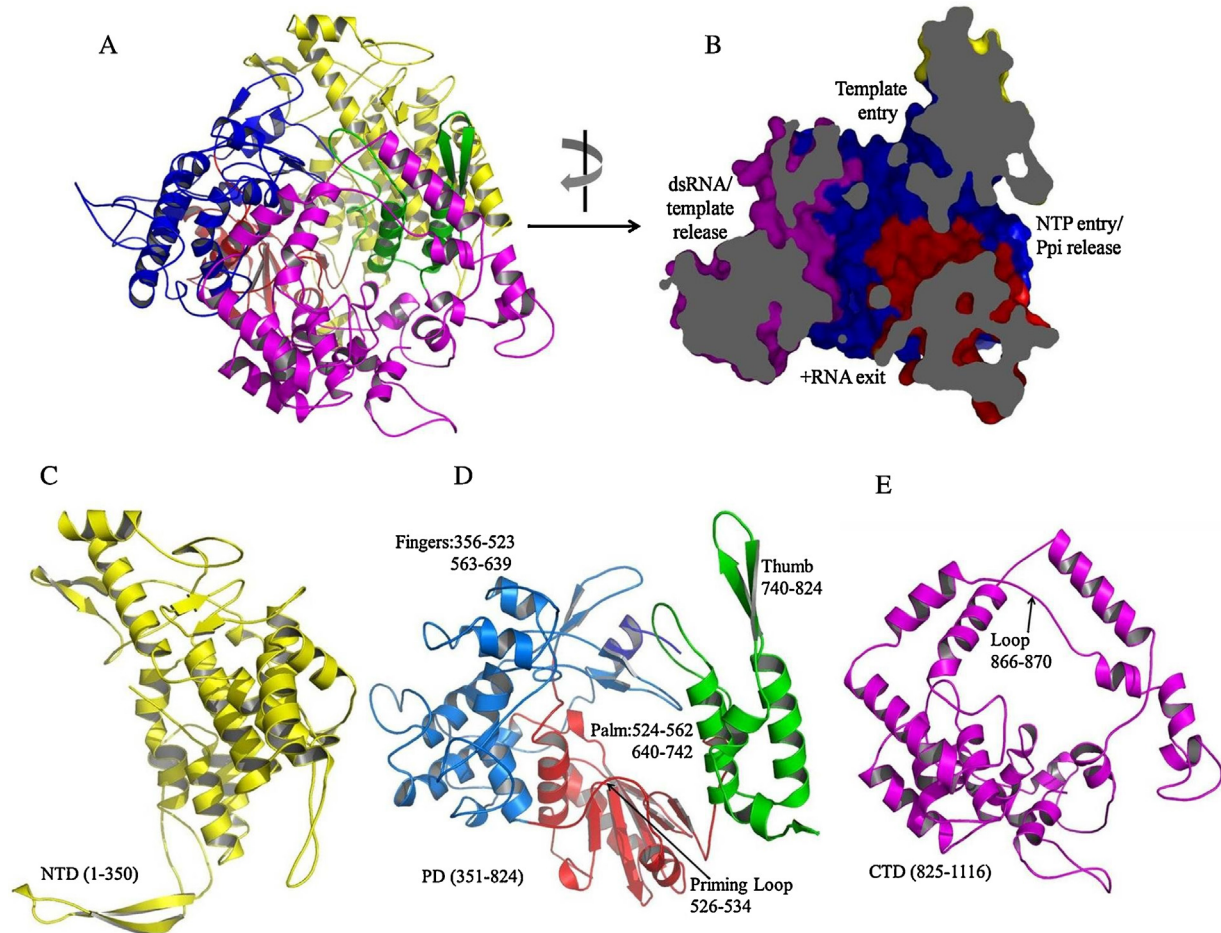


Fig. 5. Predicted structure of AmCPV RdRp, tunnels present within and its individual domains. (A) Cartoon representation of the model RdRp where region in yellow represents NTD and magenta represents CTD. Subdomains present in PD are colored as blue for finger, red for palm and green for thumb. (B) Sagittal cutaway of the surface representation of the image in (A) after 90° rotation in left. It represents predicted tunnels present within the protein. (C), (D), and (E) Cartoons represent individual domains as previously colored. (For interpretation of the references to color in this figure legend, the reader is referred to the web version of this article.)

diester bond formation between two rNTPs [21,59–61]. Mutation of D682 and/or D683 completely abrogates catalytic activity of AmCPV RdRp [15]. Motif B of the model forms a loop and α -helix structure and contains several highly conserved residues (S645, G646, T650, S651, and H654) (Fig. 3C). In case of rotavirus, HCV, PD, and RHDV the equivalent residue of H654 is asparagine while equivalent residue of S651 is a positively charged lysine residue in case of rotavirus. These residues appear to contribute in fidelity by correct nucleotide and correct template selection by analogy to other viral polymerases [21,39,62,63]. For instance, S645 may directly interact with 2'-OH group of rNTP and H654 is likely to

support proper orientation of D558 to interact with 2'-OH group of rNTP thereby helping selection of rNTP over dNTP. Primary sequence of motif D is not well conserved. However, the motif always forms α -helix, turn and short β -strand in all known RdRps and RTs except in ϕ 6 RdRp where there is an insertion of seven amino acids between the α -helix and the turn. Structural comparisons indicate that motif D may contain a hydrophilic residue at the middle of the α -helix and an aromatic residue in the following turn (Fig. 3D). The function of motif D is not yet well understood. It is presumed that the β -strand of the motif interacts with β -strand of motif A thereby stabilizing the core polymerase structure [50].

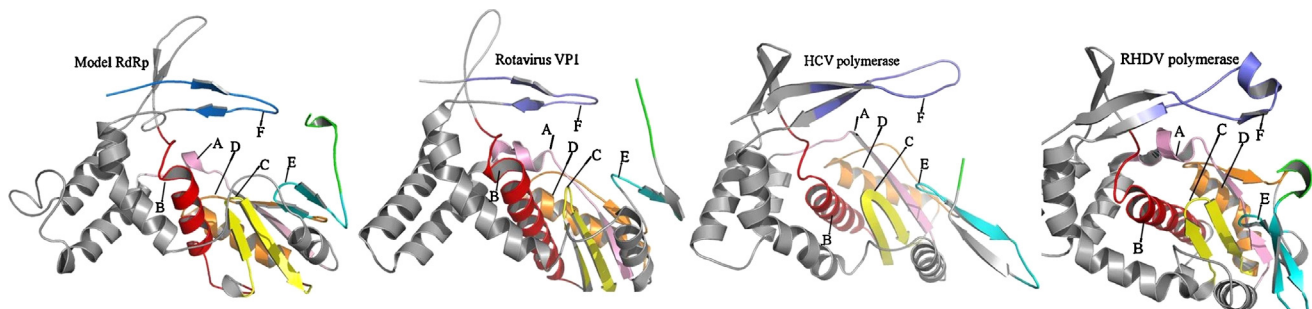


Fig. 6. Model of the polymerase domain of AmCPV RdRp and comparison of the modeled structure at the conserved motifs A–F with the solved structures of other polymerases. The motifs are colored as: motif A – pink, motif B – red, motif C – yellow, motif D – orange, and motif F – cyan.

Moreover, recent studies have extended the function of motif D in case of PV, which has shown that K359 of the flexible motif acts as general acid in two-metal ion mechanism employed by DNA/RNA polymerases [64–66]. In all known RdRPs and RTs, motif E is located at the junction of palm and thumb subdomain and is suggested to control the flexibility of the thumb subdomain [67,68]. Motif E exists in a β hairpin structure and its sequence is less conserved (Fig. 3D). Studied RdRp structures in our structural comparison with the model has identified that a hydrophilic amino acid residue (Q/K/S) may present in the first β strand and an aromatic residue (F/Y/W) following the second β strand of the β hairpin structure of motif E. The residues of motif E have been implicated in processivity and fidelity of polymerization [69]. In $\lambda 3$, L782 and K783 of motif E interact with priming nucleotide in the initiation complex [21]. The equivalent residues in the model AmCPV RdRp are L725 and Q726, which may help in positioning the priming nucleotide and are likely to contribute to the fidelity and processivity of polymerization reaction. The C-terminal portion of the palm subdomain is the thumb subdomain (residues 740–824). The sequence of the thumb subdomain is less conserved in all polymerases. The thumb subdomain of the model is of comparable size to that of $\lambda 3$, rotavirus and HCV RdRPs but considerably larger than PV and RHDV RdRp structures. Larger thumb subdomain promotes stable binding of ssRNA by the polymerases [61] to initiate *de novo* initiation in $\lambda 3$, rotavirus and HCV RdRPs and, by analogy, is likely to have similar function in the model RdRp. The flexibility of the thumb subdomain of HIV-1 RT (PDB 1RTD) is an essential attribute for nucleic acid binding and polymerization [67,70]. However, modest structural rearrangements are sufficient for RdRPs of the Reoviridae family [22]. The thumb subdomain of the model has three α -helices connected to the fourth α -helix via two anti-parallel β -strands which serve as thumb tip. R797 of $\lambda 3$ RdRp's thumb subdomain helps to stabilize the phosphate group of the priming nucleotide, and the equivalent arginine residues in the rotavirus and in the model are R690 and R740, respectively, which are expected to serve the same function.

3.2.2. N-terminal domain and C-terminal domain

The unique features of the model RdRp and other polymerases of the family Reoviridae include the presence of a large N- and a C-terminal domain, alias NTD and CTD respectively, along with a central polymerase domain (Fig. 5C–E). The globular NTD helps to maintain continuous surface between fingers and thumb subdomains thereby forming a closed structure. The C-terminal domain having an annular bracelet like structure resembles the sliding clamps of cellular RNA polymerases and forms the exit tunnel for dsRNA. There is no conserved sequence motifs have been reported for these domains. However, their overall architectures are comparable with other members though some unique structural attributes are also present among the individual members. For instance, the globular NTD is reach in α -helices in rotavirus VP1 (Lu et al. [39]) while the number of β -strands is more in case of $\lambda 3$ NTD and the model NTD. Moreover, the CTD of rotavirus VP1 is more constricted than $\lambda 3$ and the model RdRp by an α -helical plug that extends 15 Å inside the domain. The model RdRp has partially constricted CTD by a loop (residues 866–870) that is ~1.3 Å more protruding towards the corresponding dsRNA exit tunnel than the equivalent loop (residues 957–964) in $\lambda 3$ RdRp.

3.3. Surface analysis

Several differences between the surface shapes were observed among $\lambda 3$ RdRp crystal structure and AmCPV RdRp model. Superimposition of their backbones has revealed that the differences are mostly due to variability of side chains. Significant differences in surface topology were also observed among the model

and rotavirus VP1 crystal structure. This surface variability may be explained by the fact that AmCPV RdRp form complex with other viral proteins, as it is the case for $\lambda 3$ RdRp which interacts with $\mu 2$ protein or as observed in the case of rotavirus VP1 which interacts with VP2 protein. Surface amino acids have then to be specific to the viruses to allow correct interactions to the other components of the replicative complexes. The electrostatic potential comparison is presented in Fig. 7. It shows that no major prevalence of negative or positive charges can be found in any of the structures. The large positive channel near the thumb tip is supposed to guide the RNA template to the catalytic center. The dsRNA exit tunnel of the model RdRp and rotavirus RdRp is more positively charged than $\lambda 3$. The significant difference appears near the ssRNA transcript exit tunnel. The exit front of the tunnel of model RdRp is negatively charged whereas positive charge is prevalent to that of other two structurally known members. Negatively charged surface near the ssRNA transcript exit tunnel may impose a kinetic barrier to the RNA transcription process by AmCPV RdRp. Moreover, synthesis of nascent transcript followed by progress of it towards the exit tunnel may allow reorientation of some structural elements and/or amino acid side chains near the exit front of the tunnel so that a positively charged environment is created to facilitate release of negatively charged transcript.

3.4. Prediction of template RNA binding by AmCPV RdRp model

In analogy to rotavirus VP1 and $\lambda 3$ RdRp, RNA template entry tunnel has been predicted near the thumb tip in model RdRp. The tunnel is largely positively charged (Fig. 8B) by contribution of the residues from finger subdomain, C-terminal domain and the thumb subdomain. Docking of AmCPV RNA in the predicted template entry tunnel may shed light on the template recognition by AmCPV RdRp during RNA dependent RNA synthesis. RdRPs of segmented dsRNA viruses of Reoviridae family are able to synthesize RNA strand in confined proteinaceous viral core during transcription cycle and inside the cytoplasm of the host cell during replication cycle as well. Transcription process by Reoviridae RdRp recruits (−) RNA as template from dsRNA to initiate (+) RNA synthesis from the 3' end of the (−) RNA while the replication process starts from the 3' end of the (+) RNA as template to initiate (−) RNA synthesis. Extensive sequence specific interactions between Reoviridae RdRp and viral (−) RNA can be negated in case of transcription process because of two reasons: (i) there are incessant interactions among RdRp and the dsRNA genome in the confined viral core, and (ii) each viral RdRp undergoes multiple rounds of transcription using the same (−) RNA template. In contrast, improper recognition of (+) RNA by viral RdRp during virus packaging and replication may result in generation of defective progeny virus particles [32]. Hence, viral RdRp remains very strict with (+) RNA recognition signal as found in case of rotavirus VP1. Deletion of 3' conserved sequence (5'-UGUGACC-3') presents at end of the most of the rotavirus genomic mRNAs prevents rotavirus mRNAs from being served as templates for minus strand synthesis [71,72]. In case of AmCPV, analysis of sequences of its genome segments has revealed that except for a short sequence at their 3'-termini, 5'-AGACG-3', the viral mRNAs lack significant sequence identity. RNA binding property by AmCPV RdRp has also shown that the polymerase can bind with the 3' end of viral (+) RNA (~183 nucleotide) and form complex even in the presence of 25 fold or 100 fold mass excess of non-specific RNA (yeast tRNA), albeit at somewhat reduced level (Fig. 8A). Thus binding to the 3' end of viral (+) RNA is quite specific by AmCPV RdRp. Moreover, Ghorai et al. [15] has shown that AmCPV RdRp can initiate *de novo* (primer independent) (−) RNA strand synthesis from (+) RNA of S2 mini genome having intact 3' terminus conserved sequence [15]. Hence, we have predicted that this conserved sequence functions as the essential promoter region for minus strand synthesis. Docking of

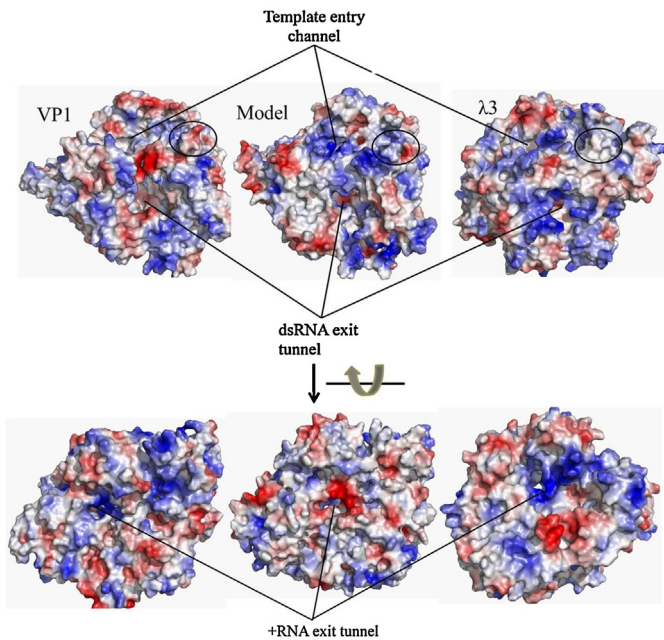


Fig. 7. Comparative analysis of electrostatic surface representation of the model along with two other representatives from Reoviridae family. They are colored according to electrostatic potential with positive in blue and negative in red. The upper panel shows the front of template entry tunnel at the vicinity of thumb subdomain (black circled) and dsRNA exit tunnel. The lower panel, derived from the upper panel upon rotation by 90° along with the axis indicated in the figure shows predicted (+) RNA exit tunnel. For interpretation of the references to color in this figure legend, the reader is referred to the web version of this article.

this conserved pentanucleotide in the template entry tunnel of the model RdRp has suggested the mode of promoter recognition by viral polymerase (Fig. 8B). The protein–RNA complex is stabilized with a large interface area between protein and RNA that measures around 1617.3 Å² as computed by Prince Web server (<http://www.princeweb.iitkgp.ernet.in/~rbahadur/prince/home.html>).

In complex, the sugar–phosphate backbone of the RNA is largely anchored against the fingers wall through extensive hydrogen bonding, leaving the RNA bases flagging outward (Fig. 8C). However, sequence specific RNA recognition is lesser in number in comparison to

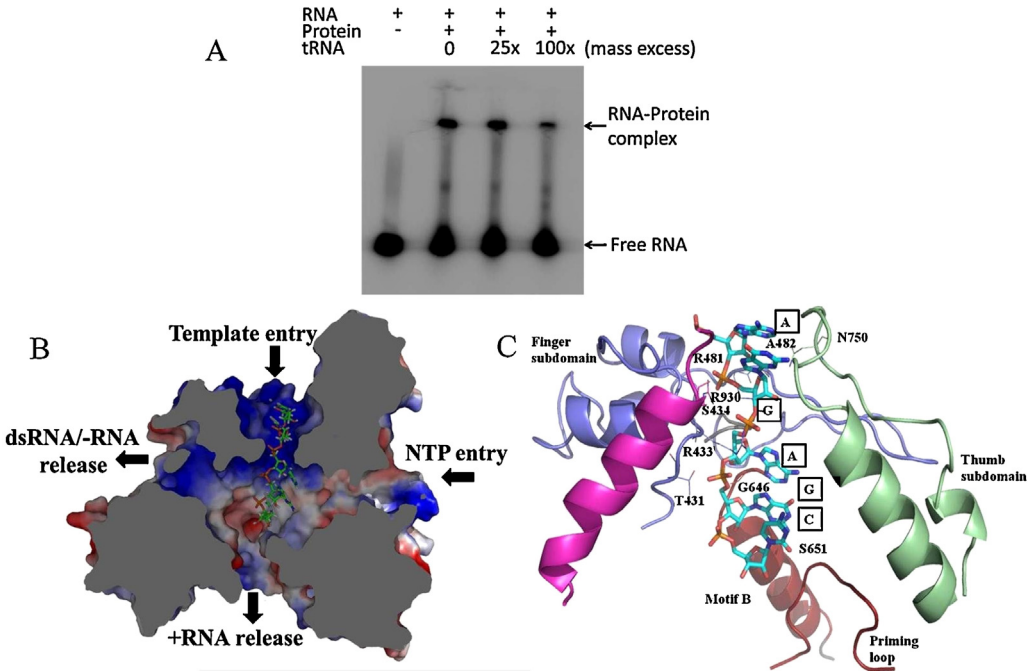


Fig. 8. AmCPV RdRp–RNA interaction. (A) Electrophoretic mobility shift assay of 3'-end of AmCPV(+) RNA alone or in the presence of purified RdRp, showing retarded mobility of RdRp–RNA complex in comparison to only RNA, and the complex can be formed even in the presence of 100 fold mass excess of non-specific RNA. (B) The image is same as Fig. 5B with the RNA pentanucleotide docked in the predicted template entry tunnel and the surface of the protein is colored as in Fig. 7. (C) Cartoon representation of the interaction where RNA bases are within square boxes and the amino acid residues involved in hydrogen bonding are represented with their side chains and residue number. The phosphate backbone of the RNA is in orange color while bases are in cyan. Portion of finger and thumb subdomains are in blue and green colors respectively and the portion of CTD are in magenta and motif B or the priming loop is in red. (For interpretation of the references to color in this figure legend, the reader is referred to the web version of this article.)

rotavirus VP1. In total of 11 hydrogen bonds, only two have been predicted to contribute in sequence specific RNA recognition. As per docking result, the pentanucleotide of AmCPV replication template may form hydrogen bonds with the residues of finger subdomain: T431, R433, S434, R481, and A482. R433 is likely to limit the passage RNA template into the predicted template entry tunnel as discussed earlier. Residues of motif B, G646 and S651, play an important role in stabilizing the 3' end of the RNA in the active site. S651 of motif B and N750 of the thumb subdomain interact with the purine ring of the guanosine residues at (*i*+1) position and the (*i*+3) position from 3'-terminus (*i*) of the pentanucleotide respectively. These interactions in together may help the RNA to sit in-register with the enzyme's active site to initiate RNA synthesis at the very end of the molecule. In case of λ3 RdRp, the equivalent residues which serve to stabilize RNA template in the active site are: T457, G460, S462, K486, K490, M515, S682, G683, and N807 [21]. However, VP1 of rotavirus has shown more sequence specific RNA binding activity than RdRps from AmCPV and λ3. The base specific recognition of RNA by rotavirus VP1 has led to the overshooting of 3'-terminal nucleotide from the active site, which needs to be repositioned properly for optimum activity [39]. Another viral protein VP2 of rotavirus is believed to be involved in repositioning the 3'-terminal nucleotide in-register with the enzyme's active site. Mutation in the base specific or sequence dependent residues (SD residues) has impaired the protein to form a stable initiation complex with 3' (+) strand CS (conserved sequence, 5'-UGUGACC-3'), thereby causing decrease in activity. However, mutation in individual SD residues has insufficient impact on dsRNA synthesis. Only, double (N186A and F416A) or triple (N186A, R190A and F416A) mutations have reduced *in vitro* dsRNA synthesis by 2-fold and 20-fold, respectively [56]. Role of sequence dependent residues (S651 and N750) of AmCPV RdRp in the recognition of conserved sequence found at the 3' termini of AmCPV (+) RNA needs to be investigated experimentally.

3.5. Molecular dynamics simulation of model RdRp and RdRp–RNA complex

An explicit solvent molecular dynamics (MD) simulation at 300 K for 10 ns has been performed using the model RdRp and RdRp–RNA complex obtained from docking experiment. Herein, the 3D structure of AmCPV RdRp model and its complex with RNA was optimized using MD simulation in solvent to mimic the real physiological environment. The stability of the only protein or the complex during the MD simulation was measured by its deviation from the initial structure in terms of RMSD and radius of gyration (R_g). The 3D-structure of model RdRp and the complex have reached equilibrium after 5 ns of simulation where RMSD of all atoms converged to 4.3 Å and 4.6 Å for the only protein and the complex respectively (Fig. 9). The radius of gyration of the systems reaches to equilibrium after a short time from the beginning of simulation and remains almost stable throughout the process (Fig. S4). The results imply a good molecular geometry of the model protein and a stable binding of the protein with RNA in its template binding site. There is no significant structural movements have been observed in the model AmCPV RdRp and its complex with RNA. It is consistent with the fact that unlike other viral polymerases which require long range conformational changes during an efficient RNA synthesis, RdRps of the Reoviridae family undergo a subtle conformational shift for template dependent *de novo* RNA synthesis. The MD simulation of the complex structure has been used to analyze variation in H-bonds formed between the protein and RNA. A two dimensional plot containing the number of H-bonds along with the simulation time is plotted (Fig. S5) and analysis has been made from 5 ns to 9 ns of the simulation time, during which the system gets maximum stability. It is observed that total number of

hydrogen bonds between protein and the RNA has been decreased in comparison to the starting structure. The lost H-bonds could be compensated by some electrostatic interactions between the charged side chains and the RNA. However, number of base specific interactions has remained almost same in our chosen time frame, although the interacting partners may be changed (data not shown). It implies that base specific interactions are required for a stable complex formation between AmCPV RdRp and viral (+) RNA, which leads to RNA dependent RNA synthesis from the very end of the RNA molecule so that all genetic information can be propagated into the progeny virus particles. The mechanism employed by φ6 replicase that ensures RNA synthesis from the very end of the template appears to be different from the members of Reoviridae family. The C-terminal domain of φ6 polymerase blocks the product exit tunnel thereby placing the 3'-terminus of the template strand in a correct position in the active site so that RNA synthesis can begin from the very end of the template molecule. The domain is expected to move away during elongation step [53].

3.6. Predicted mechanism for *de novo* RNA synthesis by AmCPV RdRp

Structure conservation among the viral RdRps is beyond their sequence similarities. It has led to a common mechanism of RNA synthesis by viral RdRps. However, in addition to obvious similarities, viral RdRps have a number of unique structural features which are important for efficient and accurate RNA dependent RNA synthesis in the different viruses. Based on available structural data, biochemical data and our docking analysis, we discuss here the predicted mechanism of *de novo* RNA dependent RNA synthesis by cypoviral RdRps in the context of AmCPV RdRp model. The prediction of *de novo* RNA synthesis is based on three major events: (i) entry of viral RNA in the polymerase active site, (ii) formation of stable initiation complex and synthesis of first phosphodiester bond, and (iii) elongation and product RNA release.

3.6.1. Entry of viral RNA in the polymerase active site

In order to propagate viral infection in the host cell, AmCPV RdRp must undergo an efficient process of recruiting viral mRNA (+RNA) or (−) RNA so that their 3'-termini are directed into the catalytic center through template entry tunnel during replication or transcription of the viral genome respectively. From the study of λ3 and rotavirus VP1, efficient recruitment of RNA (for both replication and transcription) by RdRps of Reoviridae family has been found to be dependent on at least two factors: attachment of viral mRNA with RdRp through its 5'-cap and accessibility of the 3'-terminus of (+) RNA for replication and of (−) RNA for transcription to the template entry tunnel of the replicase. Docking of N^7 -methyl-GpppG cap on the surface of the model AmCPV RdRp has predicted the protein's probable mode of mRNA cap recognition (Fig. 10A). The mRNA cap can be docked near the thumb tip of the model RdRp as found in case of λ3 and rotavirus polymerase. However, cap interacting residues are rather different for them, which is consistent with the fact that no conserved amino acids are observed for recognizing mRNA cap among λ3 and rotavirus VP1. In case of λ3, the cap can fit in a pocket located at one side of the thumb tip. Rotavirus VP1 lacks one of the two β-strands of the thumb tip, which are important for forming pocket of cap binding in λ3. However, two additional antiparallel β-strands of the N-terminal domain along with one β-strand of the thumb tip may support the VP1 cap-binding site. In model RdRp, the methylated and unmethylated guanosine rings of the docked N^7 -methyl-GpppG cap can be fitted in two separate pockets which roughly correspond to the methylated and unmethylated purine sites on λ3, respectively. Both the bases are stacked between hydrophobic residues. The positively charged methylated purine ring forms hydrogen bond with N197 of model RdRp (Fig. 10B)

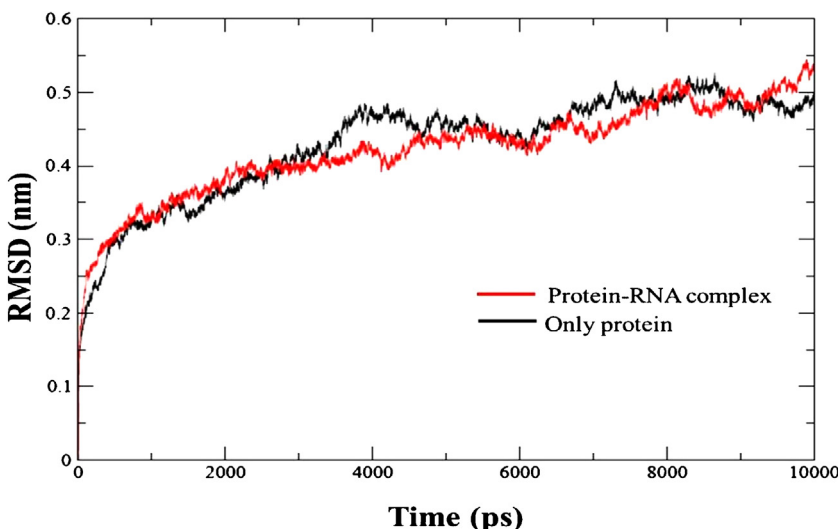


Fig. 9. Backbone C α atoms RMSD (Root-mean square deviation) relative to the initial structure along the MD trajectories (10 ns) obtained for modeled AmCPV RdRp (black) and its complex with RNA pentanucleotide (red). (For interpretation of the references to color in this figure legend, the reader is referred to the web version of this article.)

while D1035 contacts with methylated guanosine residue of the cap in case of $\lambda 3$ RdRp. This kind of cap recognition is different from vaccinia virus Vp39, the bifunctional polymerase, where the methylated purine ring is stabilized by stacking interaction from aromatic side chains and there is no pocket for unmethylated one [73]. Attachment of 5'-cap of viral mRNA may facilitate insertion of free 3' end of the negative strand into the template entry channel during transcription [21]. However, separation of negative strand from positive strand of dsRNA can be made efficient by involvement of other viral proteins as suggested in case of BTV and AmCPV [15,74]. Binding of 5'-cap at one position of the polymerase surface may also help to feed 3' end of viral mRNA into the polymerase active site during replication. As the viral genomic mRNA is fed into the active site, local genomic RNA secondary structures and any higher order RNA structures joining different genomic strands must be disrupted. As studied from cell free replication system of rotavirus [75,76] optimal secondary structure formation by viral mRNA is a favorable feature by which its 3'-terminus is made structurally appropriate for RdRp recruitment signal. We have modeled secondary structure of segment 10 (S10) genomic mRNA of AmCPV, which has predicted that residues 5 to 28 of the 5' end and residues upstream of the non-base-paired 3'-terminal stretch (residues 1075–1113) interact to form a panhandle that juxtaposes the 5' and 3' ends of the RNA (Fig. 10C). Formation of such a secondary structure leaves 3'-terminal of the mRNA having the conserved pentanucleotide (5'-AGAC-3') un-base-paired, thereby making it polymerase-accessible single stranded tail. Since only a single type of polymerase is responsible for synthesis of all the dsRNA genome segments, the various genomic mRNA templates may be predicted to share a common mechanism of RdRp recruitment process. Once the 3' end of viral RNA reaches in the vicinity of the template entry tunnel, it approaches towards the catalytic center through base specific and/or non-specific interaction of the RNA with the polymerase residues. Unlike rotavirus VP1, such interactions may help the RNA to sit in-register with the enzyme's active site as in case of $\lambda 3$ RdRp. Being active without the involvement of any other viral proteins, we can predict that AmCPV RdRp also gets an in-register template strand in its catalytic center (as discussed in Section 3.4).

3.6.2. Formation of stable initiation complex and synthesis of first phosphodiester bond

Superimposition of the model polymerase domain with the initiation complex and short elongationcomplex of $\lambda 3$ RdRp (PDB

1N1H and 1N38 respectively) along with the comparison with other viral polymerases have guided us to identify important residues involved in the condensation reaction between two initiation rNTPs in the catalytic center of the model, thereby predicting plausible mechanism of *de novo* initiation of RNA synthesis by AmCPV RdRp. When the rNTPs and the template approach through the rNTP tunnel and the template tunnel respectively, they arrive at the catalytic site for forming a *de novo* initiation complex. The first rNTP or the priming nucleotide is the first nucleotide of the nascent RNA strand and is complementarily base paired to the very last base (i) of the template strand. A second rNTP molecule comes at the position of ($i+1$) of the template and interacts with the template base through Watson–Crick base pairing. Several residues of the polymerase are involved in stabilizing these two nucleotides in their proper positions and facilitate first phosphodiester bond formation between them. For the members of Reoviridae family, priming loop is supposed to stabilize these two nucleotides from bottom. However, in case of rotavirus VP1, the loop (residues 489–499) is in retracted position incapable of supporting the priming nucleotide. Priming loop of $\lambda 3$ (residues 557–566) hydrogen bonds with the phosphate group of the initiation nucleotide through S561 and K566 and their structurally equivalent residues (G531 and D534) of the model priming loop (residues 526–534) are likely to involve in the same function. In the model structure, several other residues from motifs A–C, F, E and thumb subdomains may function in stabilization of the rNTPs as discussed earlier (Section 3.2.1). Once the two nucleotides are in their catalytically favorable position, phosphodiester bond formation is initiated by a nucleophilic attack from deprotonated 3'-OH of the sugar moiety of initiation nucleotide to the α -phosphate of the second nucleotide. All known polymerases are evolved to use two metal ions (usually Mg $^{2+}$) for their activity [61]. First metal ion helps deprotonation of the 3'-OH group for the in line nucleophilic attack. Second metal ion helps proper orientation of the triphosphate moiety of the second nucleotide and stabilizes negative charges arise during pentavalent transition state. In analogy to two metal ion mechanism employed by all known DNA/RNA polymerases, possible mechanism of nucleotidyl transfer reaction has been proposed for AmCPV RdRp and it is depicted in Fig. 11. Each of the metal ions is expected to form the octahedral geometry with the polymerase residues, triphosphate moiety and water molecule(s) during the formation of pentavalent transition state. Recent studies on PV, foot-and-mouth disease virus (FMDV), Norwalk virus (NV), human rhinovirus (HRV) and human immunodeficiency virus type 1 (HIV 1) have proposed that a con-

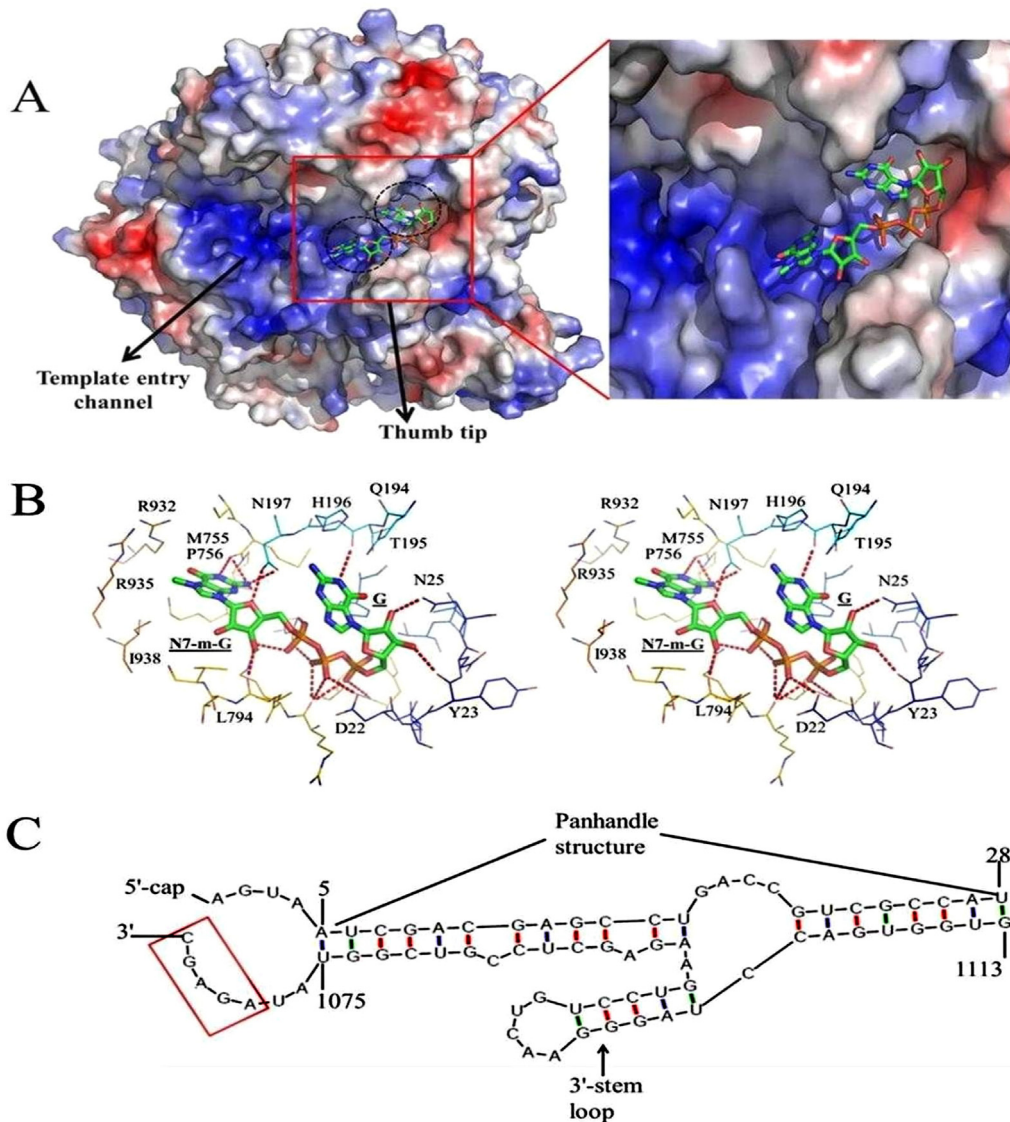


Fig. 10. Interaction of mRNA cap with model AmCPV RdRp and its role in template feeding. (A) Docking of N7-m-GpppG cap on the surface of the protein shows its location at one side of the thumb and near the template entry tunnel. Phosphate backbone of the cap is in orange color while the bases are green. Two separate pockets for methylated and unmethylated guanosine residues are indicated by dotted circles and color of the protein surface is same as in Fig. 7. (B) Wall-eyed stereo view of the mRNA cap binding pocket which is in the same orientation as in (A). Hydrogen bonds are represented in red dotted lines. (C) Portion of the predicted secondary structure of S10 genomic mRNA. Important features include the panhandle structure, 3'-stem loop and un-base-paired 5' and 3'-ends. The conserved pentanucleotide at the 3'-end is within red box. mRNA cap present at the un-base-paired 5'-end interacts with AmCPV RdRp thereby help in feeding of the 3'-end of the template RNA into the catalytic center. (For interpretation of the references to color in this figure legend, the reader is referred to the web version of this article.)

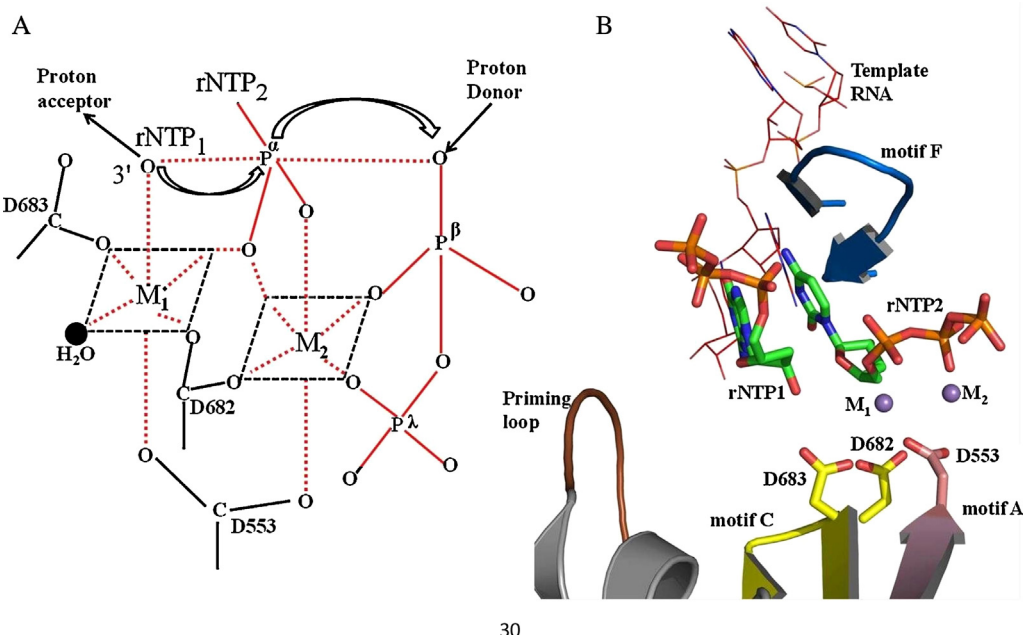
served lysine residue of motif D is involved as a general acid for protonation of the β -phosphate thereby making it better leaving group. Further, conformational flexibility of motif D is an inevitable issue in order to bring it into proper catalytic register.

However, members of the Reoviridae family have limited flexibility in their overall RdRp structure and residue acts as general acid not yet reported, though in the absence of any general acid, water molecule may serve for the same [64]. A productive initiation often leads to elongation step of RNA synthesis by viral RdRps.

3.6.3. Elongation and product RNA release

Comparison of our model structure with short (PDB 1N38) and long elongation complexes (1N35) of $\lambda 3$ RdRp may shed light on the prediction of elongation and product release step for AmCPV RdRp. Upon successive addition of rNTPs, nucleotidyl reaction is repeated until the polymerase finishes copying the template. During productive elongation step, the priming loop has to be retracted towards

the palm subdomain otherwise abortive initiation may be resulted as suggested for $\lambda 3$ RdRp. For $\lambda 3$ structure, the duplex RNA product has to bend and follow the dsRNA exit tunnel, unless the duplex may collide with a loop (residues 1109–1125) that is suggested to force the RNA synthesis process in the transcriptional mode where the nascent ssRNA gets separated from template strand and approaches through the (+) RNA exit tunnel. Secondary factor for the strand separation may come from another loop (residues 957–964) of the C-terminal domain. The equivalent structure of this loop in the model corresponds to the residues 866–870 and is $\sim 1.3 \text{ \AA}$ more protruding towards the dsRNA exit tunnel thereby making it partially obstructed (Fig. 12). This structural attribute of the model RdRp may be able to explain why recombinant AmCPV RdRp performs RNA synthesis in the transcriptional mode *in vitro* [15] while recombinant rotavirus and BTV replicases are reported to synthesize dsRNA product in *in vitro* condition. Interactions with other viral proteins may be expected for AmCPV RdRp, which are required for switch-



30

Fig. 11. Prediction of nucleotidyl transfer reaction employed by AmCPV RdRp. (A) Schematic representation of two metal ion mechanism adopted from Castro et al. [64]. First metal ion (M_1) is predicted to form octahedral geometry with 3'-OH of rNTP₁, D682 and D683 of motif C, one water molecule and α -phosphate group of rNTP₂ while the second metal ion (M_2) is predicted to form the same with D553 of motif A, D682 of motif C and α , β , and λ -phosphate molecules of rNTP₂. Nucleophilic attack by deprotonated 3'-OH group of rNTP₁ to the α -phosphate moiety of rNTP₂ is followed by bond breakage between α -phosphate and β -phosphate moiety of rNTP₂ (shown by curved arrow). Non-covalent interactions are indicated by dotted line while covalent interactions are in solid line. (B) Position of the catalytic residues in AmCPV RdRp is represented by cartoon structures as obtained from superimposition of the model structure with the initiation complex of $\lambda 3$ RdRp (PDB 1N1H).

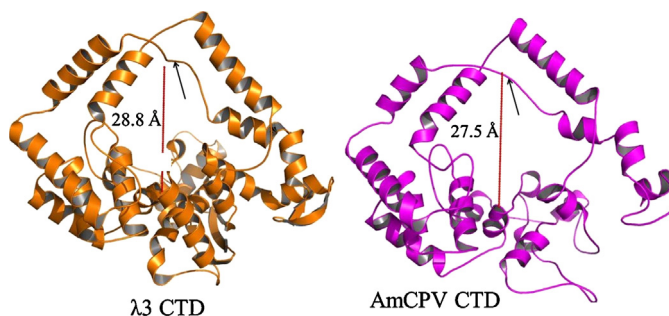


Fig. 12. Comparative structural analysis of CTDs from $\lambda 3$ RdRp (PDB 1N35) and the model RdRp. Position of a loop (residues 957–964) in $\lambda 3$ CTD is shown by a black arrow, which is predicted to be involved in strand separation. The equivalent structural element in the model corresponds to the residues 866–870 also marked by black arrow. Distance of the loop from the base of the CTD is 28.8 Å and 27.5 Å for $\lambda 3$ and the model, respectively, indicated by red dotted line. For the model the distance is measured between $C\alpha$ residues of Q866 and M1066 while for $\lambda 3$, G959 and V1176 were considered for distance measurement. Q866–G959 and M1066–V1176 are two structurally equivalent amino acid pairs for the model and $\lambda 3$. (For interpretation of the references to color in this figure legend, the reader is referred to the web version of this article.)

ing the polymerase into replication mode during the packaging of virus progeny particles.

4. Conclusion

Despite lack of substantial sequence similarity between AmCPV RdRp and other structurally known polymerases, we have been able to model the three dimensional structure of AmCPV RdRp. In the absence of any structural data, this model and our docking analysis allow prediction of functions of the conserved residues and motifs thereby suggesting possible mechanism of RNA dependent RNA synthesis by the enzyme. Moreover, it has helped to explain the structural basis of biochemical results as we had reported previously. These information in together should be helpful in designing anti-AmCPV compounds as well as provide guidance for future biochemical experiments.

Acknowledgements

The work is supported by a grant from Department of Science and Technology, Govt. of India (No: SR/SO/BB-0038/2011). AK, AD, and PB thank IIT Kharagpur, DBT (GOI) and ICMR (GOI), respectively, for providing research fellowship.

Appendix A. Supplementary data

Supplementary data associated with this article can be found, in the online version, at <http://dx.doi.org/10.1016/j.jmgm.2015.07.002>

References

- [1] M.S. Jolly, S.K. Sen, M.M. Ahsan, *Tasar Culture*, Ambika Publishers, Bombay, India, 1974.

- [2] P.P.C. Mertens, S. Rao, Z.H. Zhou, Cypovirus, in: C.M. Fauquet, M.A. Mayo, J. Maniloff, U. Desselberger, L.A. Ball (Eds.), *Virus Taxonomy. 8th Report of the ICTV*, Elsevier Academic Press, Amsterdam etc, 2005, pp. 522–533.
- [3] C.C. Payne, P.P.C. Mertens, Cytoplasmic polyhedrosis viruses, in: W.K. Joklik (Eds.), *The Reoviridae*, Plenum, New York, 1983, pp. 425–504.
- [4] S. Rao, G. Carner, R. Shapiro, S.W. Scoot, T. Omura, K. Hagiwara, Comparison of the amino acid sequences of RNA dependent RNA polymerases of cypoviruses in the family Reoviridae, *Arch. Virol.* 148 (2003) 209–219.
- [5] M. Arella, C. Lavallee, S. Bellonci, Y. Furuchi, Molecular cloning and characterization of cytoplasmic polyhedrosis virus polyhedrin and a viable deletion mutant gene, *J. Virol.* 62 (1988) 211–217.
- [6] K.R. Qanungo, S.C. Kundu, A.K. Ghosh, Characterization of cypovirus isolates from tropical and temperate Indian saturniidae silkworms, *Acta Virol.* 44 (2000) 349–357.
- [7] M. Chakrabarti, S. Ghorai, S.K.K. Mani, A.K. Ghosh, Molecular characterization of genome segments 1 and 3 encoding two capsid proteins of *Antherea mylitta* cytoplasmic polyhedrosis virus, *J. Virol.* 7 (2010) 181–191.
- [8] V.R. Chavali, A.K. Ghosh, Molecular cloning, sequence analysis and expression of genome segment 7(S7) of *Antherea mylitta* cypovirus (AmCPV) that encodes a viral structural protein, *Virus Genes* 35 (2007) 433–441.
- [9] V.R. Chavali, C. Madhurantakam, S. Ghorai, S. Roy, A.K. Das, A.K. Ghosh, Genome segment 6 of *Antherea mylitta* cypovirus encodes a structural protein with ATPase activity, *Virology* 377 (2008) 7–18.
- [10] S.R. Jangam, M. Chakrabarti, A.K. Ghosh, Molecular cloning, expression and analysis of *Antherea mylitta* cypovirus genome segments 8 and 11, *Int. J. Virol.* 3 (2006) 60–72.
- [11] K.R. Qanungo, S.C. Kundu, J.I. Mullins, A.K. Ghosh, Molecular cloning and characterization of *Antherea mylitta* cytoplasmic polyhedrosis virus genome segment 9, *J. Gen. Virol.* 83 (2002) 1483–1491.
- [12] U. Sinha-Datta, V.R. Chavali, A.K. Ghosh, Molecular cloning and characterization of *Antherea mylitta* cytoplasmic polyhedrosis virus polyhedrin gene and its variant forms, *Biochem. Biophys. Res. Commun.* 332 (2005) 710–718.
- [13] P. Biswas, A. Kundu, A.K. Ghosh, Genome segment 4 of *Antherea mylitta* cytoplasmic polyhedrosis virus encodes RNA triphosphatase and methyltransferases, *J. Gen. Virol.* 96 (2015) 95–105.
- [14] P. Biswas, A. Kundu, A.K. Ghosh, Genome segment 5 of *Antherea mylitta* cytoplasmic polyhedrosis virus encodes a bona fide guanylyltransferase, *J. Virol.* 88 (2014) 1–13.
- [15] S. Ghorai, M. Chakrabarti, S. Roy, V.R. Chavali, A. Bagchi, A.K. Ghosh, Molecular characterization of genome segment 2 encoding RNA dependent RNA polymerase of *Antherea mylitta* cytoplasmic polyhedrosis virus, *Virology* 404 (2010) 21–31.
- [16] P. Ahlquist, Parallels among positive-strand RNA viruses, reverse-transcribing viruses and double-stranded RNA viruses, *Nat. Rev. Microbiol.* 4 (2006) 371–382.
- [17] S.D. Trask, S.M. McDonald, J.T. Patton, Structural insights into the coupling of virion assembly and rotavirus replication, *Nat. Rev. Microbiol.* 10 (2012) 165–177.
- [18] X. Zhang, S.B. Walker, P.R. Chipman, M.L. Nibert, T.S. Baker, Reovirus polymerase 3 localized by cryo-electron microscopy of virions at a resolution of 7.6 Å, *Nat. Struct. Biol.* 10 (2003) 1011–1018.
- [19] L.F. Estrozi, E.C. Settembre, G. Goret, B. McClain, X. Zhang, J.H. Chen, N. Grigorieff, S.C. Harrison, Location of the dsRNA-dependent polymerase VP1, in rotavirus particles, *J. Mol. Biol.* 425 (2013) 124–132.
- [20] S.M. McDonald, RNA synthetic mechanisms employed by diverse families of RNA viruses, *Wiley Interdiscip. Rev. RNA* 4 (2013) 351–367.
- [21] Y. Tao, D.L. Farsetta, M.L. Nibert, S.C. Harrison, RNA synthesis in a cage-structural studies of reovirus polymerase lambda3, *Cell* 111 (2001) 733–745.
- [22] S.M. McDonald, Y.J. Tao, J.T. Patton, The ins and outs of four-tunneled Reoviridae RNA-dependent RNA polymerases, *Curr. Opin. Struct. Biol.* 19 (2009) 775–782.
- [23] M. Boyce, J. Wehrfritz, R. Noad, P. Roy, Purified recombinant bluetongue virus VP1 exhibits RNA replicase activity, *J. Virol.* 78 (2004) 3994–4002.
- [24] J.M. Wehrfritz, M. Boyce, S. Mirza, P. Roy, Reconstitution of bluetongue virus polymerase activity from isolated domains based on a three-dimensional structural model, *Biopolymers* 86 (2007) 83–94.
- [25] M.H.V. Regenmortel, C.M. Fauquet, D.H.L. Bishop, E.B. Carstens, M.K. Estes, S.M. Lemon, J. Maniloff, M.A. Mayo, D.J. McGeoch, C.R. Pringle, R.B. Wickner, *Virus Taxonomy*, Academic Press, San Diego, 2000.
- [26] C.L. Hill, T.F. Booth, B.V. Prasad, J.M. Grimes, P.P. Mertens, G.C. Sutton, D.I. Stuart, The structure of a cypovirus and the functional organization of dsRNA viruses, *Nat. Struct. Biol.* 6 (1999) 565–568.
- [27] H. Zhang, J. Zhang, X. Yu, X. Lu, Q. Zhang, J. Jakana, D.H. Chen, X. Zhang, Z.H. Zhou, Visualization of protein–RNA interactions in cytoplasmic polyhedrosis virus, *J. Virol.* 73 (1999) 1624–1629.
- [28] Z.H. Zhou, H. Zhang, J. Jakana, X.Y. Lu, J.Q. Zhang, Cytoplasmic polyhedrosis virus structure at 8 Å by electron cryomicroscopy: structural basis of capsid stability and mRNA processing regulation, *Structure* 11 (2003) 651–663.
- [29] L. Cheng, J. Sun, K. Zhang, Z. Mou, X. Huang, G. Ji, F. Sun, J. Zhang, P. Zhu, Atomic model of a cypovirus built from cryo-EM structure provides insight into the mechanism of mRNA capping, *Proc. Natl. Acad. Sci. U. S. A.* 108 (2011) 1373–1378.
- [30] C. Yang, G. Ji, H. Liu, K. Zhang, G. Liu, F. Sun, P. Zhu, L. Cheng, Cryo-EM structure of a transcribing cypovirus, *Proc. Natl. Acad. Sci. U. S. A.* 109 (2012) 6118–6123.
- [31] B. Zhu, C. Yang, H. Liu, L. Cheng, F. Song, S. Zeng, X. Huang, G. Ji, P. Zhu, Identification of the active sites in the methyltransferases of a transcribing dsRNA virus, *J. Mol. Biol.* 426 (2014) 2167–2174.
- [32] J.T. Patton, E. Spencer, Genome replication and packaging of segmented double-stranded RNA viruses, *Virology* 277 (2000) 217–225.
- [33] S.M. McDonald, J.T. Patton, Assortment and packaging of the segmented rotavirus genome, *Trends Microbiol.* 19 (2011) 136–144.
- [34] Y. Zhang, I-TASSER server for protein 3D structure prediction, *BMC Bioinf.* 9 (2008) 40.
- [35] A. Sali, T.L. Blundell, Comparative protein modelling by satisfaction of spatial restraints, *J. Mol. Biol.* 234 (1993) 779–815.
- [36] P. Emsley, B. Lohkamp, W.G. Scot, K. Cowtan, Features and development of Coot, *Acta Crystallogr. D Biol. Crystallogr.* 66 (2010) 486–501.
- [37] R.A. Laskowski, M.W. MacArthur, D.S. Moss, J.M. Thornton, PROCHECK – a program to check the stereochemical quality of protein structures, *J. Appl. Cryst.* 26 (1993) 283–291.
- [38] O. Trott, A.J. Olson, AutoDock vina: improving the speed and accuracy of docking with a new scoring function, efficient optimization and multithreading, *J. Comput. Chem.* 31 (2010) 455–461.
- [39] X. Lu, S.M. McDonald, M.A. Tortorici, Y.J. Tao, R. Vasquez-Del Carpio, M.L. Nibert, J.T. Patton, S.C. Harrison, Mechanism for coordinated RNA packaging and genome replication by rotavirus polymerase VP1, *Structure* 16 (2008) 1678–1688.
- [40] M. Zuker, Mfold web server for nucleic acid folding and hybridization prediction, *Nucleic Acids Res.* 31 (2003) 3406–3415.
- [41] D.W. Ritchie, High order analytic translation matrix elements for real space six-dimensional polar fourier correlations, *J. Appl. Cryst.* 38 (2005) 808–818.
- [42] D. van der Spoel, E. Lindahl, B. Hess, G. Groenhof, A.E. Mark, H.J.C. Berendsen, GROMACS: fast, flexible and free, *J. Comp. Chem.* 26 (2005) 1701–1718.
- [43] W.D. Cornell, P. Cieplak, C.I. Bayly, I.R. Gould, M. Kenneth, J. Merz, D.M. Ferguson, D.C. Spellmeyer, T. Fox, J.W. Caldwell, P.A. Kollman, A second generation force field for the simulation of proteins, nucleic acids and organic molecules, *J. Am. Chem. Soc.* 117 (1995) 5179–5197.
- [44] W.L. Jorgensen, J. Chandrasekhar, J.D. Madura, R.W. Impey, M.L. Klein, Comparison of simple potential functions for simulating liquid water, *J. Chem. Phys.* 79 (1983) 926–935.
- [45] H.J.C. Berendsen, J.P.M. Postma, W.F. van Gusteren, A. Di Nola, J.R. Haak, Molecular dynamics with coupling to an external bath, *J. Comput. Phys.* 81 (1984) 3684–3690.
- [46] M. Parrinello, A. Rahman, Polymorphic transitions in single-crystals – a new molecular-dynamics method, *J. Appl. Phys.* 52 (1981) 7182–7190.
- [47] T. Darden, D. York, L. Pedersen, Particle mesh Ewald-an $N \log(n)$ method for Ewald sums in large systems, *J. Chem. Phys.* 98 (1993) 10089–10092.
- [48] B. Hess, H. Bekker, H.J.C. Berendsen, J.E.G.M. Fraaije, LINCS: a linear constraint solver for molecular simulations, *J. Comput. Chem.* 18 (1997) 1463–1472.
- [49] E.K. O'Reilly, C.C. Kao, Analysis of RNA-dependent RNA polymerase structure and function as guided by known polymerase structures and computer predictions of secondary structure, *Virology* 252 (1998) 287–303.
- [50] X. Xu, Y. Liu, S. Weiss, E. Arnold, S.G. Sarafianos, J. Ding, Molecular model of SARS coronavirus polymerase: implications for biochemical functions and drug design, *Nucleic Acids Res.* 31 (2003) 7117–7130.
- [51] J.A. Bruenn, A structural and primary sequence comparison of the viral RNA-dependent RNA polymerases, *Nucleic Acids Res.* 31 (2003) 1821–1829.
- [52] S. Bressanelli, L. Tomei, F.A. Rey, R. De Francesco, Structural analysis of the hepatitis C virus RNA polymerase in complex with ribonucleotides, *J. Virol.* 76 (2002) 3482–3492.
- [53] S.J. Butcher, J.M. Grimes, E.V. Makeyev, D.H. Bamford, D.I. Stuart, A mechanism for initiating RNA-dependent RNA polymerization, *Nature* 410 (2001) 235–240.
- [54] S. Bressanelli, L. Tomei, A. Roussel, I. Incitti, R.L. Vitale, M. Mathieu, R. De Francesco, F.A. Rey, Crystal structure of the RNA dependent RNA polymerase of hepatitis C virus, *Proc. Natl. Acad. Sci. U. S. A.* 96 (1999) 13034–13039.
- [55] C.A. Lesburg, M.B. Cable, E. Ferrari, Z. Hong, A.F. Mannarino, P.C. Weber, Crystal structure of the RNA-dependent RNA polymerase from hepatitis C virus reveals a fully encircled active site, *Nat. Struct. Biol.* 6 (1999) 937–943.
- [56] K.M. Ogden, H.N. Ramanathan, J.T. Patton, Residues of the rotavirus RNA-dependent RNA polymerase template entry tunnel that mediate RNA recognition and genome replication, *J. Virol.* 85 (2011) 1958–1969.
- [57] O. Poch, I. Sauvaget, M. Delarue, N. Tordo, Identification of four conserved motifs among the RNA-dependent polymerase encoding elements, *EMBO J.* 8 (1989) 3867–3874.
- [58] J. Pan, V.N. Valkharia, Y.J. Tao, The structure of a birnavirus polymerase reveals a distinct active site topology, *Proc. Natl. Acad. Sci. U. S. A.* 104 (2007) 7385–7390.
- [59] J.L. Hansen, A.M. Long, S.C. Schultz, Structure of the RNA dependent RNA polymerase of poliovirus, *Structure* 5 (1997) 1109–1122.
- [60] D.W. Gohara, S. Crotty, J.J. Arnold, J.D. Yoder, R. Andino, C.E. Cameron, Poliovirus RNA-dependent RNA polymerase (3Dpol): structural, biochemical and biological analysis of conserved structural motifs A and B, *J. Biol. Chem.* 275 (2000) 25523–25532.
- [61] D. Boehr, J.J. Arnold, I.M. Moustafa, C.E. Cameron, Structure, dynamics, and fidelity of RNA-dependent RNA polymerases, in: K.S. Murakami, M.A.

- Trakselis (Eds.), Nucleic Acid Polymerases, Nucleic Acids and Molecular Biology, vol. 30, Springer-Verlag, Berlin, Heidelberg, 2014, pp. 309–333.
- [62] H. Ago, T. Adachi, A. Yoshida, M. Yamamoto, N. Habuka, K. Yatsunami, M. Miyano, Crystal structure of the RNA dependent RNA polymerase of hepatitis C virus, *Structure* 7 (1999) 1417–1426.
- [63] K.K. Ng, M.M. Cherney, A.L. Vazquez, A. Machin, J.M. Alonso, F. Parra, M.N. James, Crystal structures of active and inactive conformations of a caliciviral RNA-dependent RNA polymerase, *J. Biol. Chem.* 277 (2002) 1381–1387.
- [64] C. Castro, E.D. Smidansky, J.J. Arnold, K.R. Maksimchuk, I. Moustafa, A. Uchida, M. Götte, W. Konigsberg, C.E. Cameron, Nucleic acid polymerases use a general acid for nucleotidyl transfer, *Nat. Struct. Mol. Biol.* 16 (2009) 212–218.
- [65] H. Shen, H. Sun, G. Li, What is the role of motif D in the nucleotide incorporation catalyzed by the RNA-dependent RNA polymerase from poliovirus, *PLoS Comput. Biol.* 8 (2012) e1002851, <http://dx.doi.org/10.1371/journal.pcbi.1002851>
- [66] C.E. Cameron, I.M. Moustafa, J.J. Arnold, Dynamics: the missing link between structure and function of the viral RNA-dependent RNA polymerase, *Curr. Opin. Struct. Biol.* 19 (2009) 768–774.
- [67] H. Huang, R. Chopra, G.L. Verdine, S.C. Harrison, Structure of a covalently trapped catalytic complex of HIV-1 reverse transcriptase: implications for drug resistance, *Science* 282 (1998) 1669–1675.
- [68] A. Jacobo-Molina, J. Ding, R.G. Nanni, A.D. Clark Jr., X. Lu, C. Tantillo, R.L. Williams, G. Kamer, A.L. Ferris, P. Clark, et al., Crystal structure of human immunodeficiency virus type 1 reverse transcriptase complexed with double-stranded DNA at 3 Å resolution shows bent DNA, *Proc. Natl. Acad. Sci. U. S. A.* 90 (1993) 6320–6324.
- [69] M. Gutierrez-Rivas, L. Menendez-Arias, A mutation in the primer grip region of HIV-1 reverse transcriptase that confers reduced fidelity of DNA synthesis, *Nucleic Acids Res.* 29 (2001) 4963–4972.
- [70] J. Ding, K. Das, Y. Hsiou, S.G. Sarafianos, J.A.D. Clark, A. Jacobo-Molina, C. Tantillo, S.H. Hughes, E. Arnold, Structure and functional implications of the polymerase active site region in a complex of HIV-1 RT with double-stranded DNA and an antibody Fab fragment at 2.8 Å resolution, *J. Mol. Biol.* 284 (1998) 1095–1111.
- [71] J.T. Patton, M.J. Wentz, X. Jiang, R.F. Ramig, Cis-acting signals that promote genome replication in rotavirus mRNAs, *J. Virol.* 70 (1996) 3961–3971.
- [72] M.J. Wentz, J.T. Patton, R.F. Ramig, The 39-terminal consensus sequence of rotavirus mRNA is the minimal promoter of negative strand RNA synthesis, *J. Virol.* 70 (1996) 7833–7841.
- [73] A.E. Hodel, P.D. Gershon, X. Shi, F.A. Quiocio, The 1.85 Å structure of vaccinia protein VP39: a bifunctional enzyme that participates in the modification of both mRNA ends, *Cell* 85 (1996) 247–256.
- [74] N. Stauber, J. Martinez Costas, G. Sutton, K. Monastyrskaya, P. Roy, Bluetongue virus VP6 protein binds ATP and exhibits an RNA-dependent ATPase function and a helicase activity that catalyze the unwinding of double-stranded RNA substrates, *J. Virol.* 71 (1997) 7220–7226.
- [75] D. Chen, J.T. Patton, Rotavirus RNA replication requires a single-stranded 3' end for efficient minus-strand synthesis, *J. Virol.* 72 (1998) 7387–7396.
- [76] M.A. Tortorici, B.A. Shapiro, J.T. Patton, A base-specific recognition signal in the 5' consensus sequence of rotavirus plus-strand RNAs promotes replication of the double-stranded RNA genome segments, *RNA* 12 (2006) 133–146.